(Section A: Planning Strategies and Design Concepts)

著者	Zhan Qingming, Fan Yuli, Xiao Yinghui, Ouyang Wanlu, Lan Yuliang, Yin Jie
著者別表示	Zhang Li
journal or publication title	International Review for Spatial Planning and Sustainable Development
volume	6
number	4
page range	148-164
year	2018-10-15
URL	http://doi.org/10.24517/00053272

doi: 10.14246/irspsd.6.4_148

International review for spatial planning and sustainable development A: Planning Strategies and Design Concept, Vol.6, No.4, 148-164
ISSN: 2187-3666 (online)
DOI: http://dx.doi.org/10.14246/irspsda.6.4_148

Sustainable Strategy: Comprehensive Computational Approach for Wind Path Planning in Dense Urban Area

Qingming Zhan[1,2,3*], Yuli Fan[1,2],Yinghui Xiao[1,3], Wanlu Ouyang[1,3], Yuliang Lan[1,3], Zhicheng Jin[2,3], JieYin[1,3], Li Zhang[1,3]
1 School of Urban Design, Wuhan University
2 School of Remote Sensing and Information Engineering, Wuhan University
3 Collaborative Innovation Center of Geospatial Technology
** Corresponding Author, Email: qmzhan@whu.edu.cn*

Received: Apr 5, 2018; Accepted: Aug 27, 2018

Key words: Urban heat environment, Computational fluid dynamics, Weather research and forecast, Local climate zones, Remote sensing

Abstract: This paper introduces a comprehensive framework that assesses the urban heat environment and formulates urban wind paths. Compared with other ecosystems, the wind environment and heat environment in urban areas can be much more complicated and dynamic. Nonetheless, it is of great concern considering the agglomerated population and industries at stake. Hence, multiple computational techniques are developed to assess the contemporary heat environment, and to formulate feasible policies to improve it to a more liveable state by introducing the solution of natural wind. Three key factors are considered: solar radiation, which is the major source of heat; wind direction and wind speed, which transports heat in space; and urban land surface, which may affect radiation reflection, contain auxiliary heat sources or cause vertical air flow. Hence, mesoscale meteorological data are applied to provide information about solar radiation, and are used for simulating local wind flow; Landsat images can be translated into land surface temperature figures; and building and land use databases provide information about built-up features. These combined, the local heat environment in urban areas can be mapped and monitored in a periodic fashion, with wind path analysis providing possibilities in cooling down the hotspots. Practices in cities including Fuzhou and Wuhan have proved constructive, with some others still underway.

1. INTRODUCTION

1.1 Urban heat environment and wind paths

The deterioration of the urban heat environment has had severe social and economic consequences, including human casualties, equipment dysfunction and others (Medina-Ramón et al., 2006). Though partially a result of global climate change (Luber & McGeehin, 2008), this phenomenon is also largely caused by the change of impervious surface, change of land use, urban traffic, decreasing water bodies, and other factors closely related to local human activities that can be regulated by policy and engineering efforts (Golden, 2004 ; Xu, 2010).

Correspondingly, many researchers are digging into the relationship of surface-air temperature and urban construction. Early investigations included the analysis of static surface heat patterns in Shanghai (Chen et al., 2002), and studies on dynamic changes and change simulation were introduced later (Xue, 2007; Feng et al., 2016). A comprehensive measurement for local response to solar radiation, known as Local Climate Zones, was introduced in 2012 (Stewart & Oke, 2012); the tool was later applied to both empirical research and policy studies (J Wang, Zhan, & Xiao, 2015; Cai et al., 2018).

Other researchers have focused on the possible use of wind to disperse heat from local heat islands. Such studies date back to the 1990s (Ishida, Tsumura, & Takagi, 1997) , and were followed by studies on Hongkong, Taiwan, Wrocaw, Cologne, and Szeged. These studies analyze natural wind paths through cities using meteorological models, such as Weather Research and Forecast (WRF) and the Regional Boundary Layer Model (RBLM), and rely on spatial policies to ensure the availability of the passage (Li & Rong, 2014). Simulations at the street block scale with Computational Fluid Dynamics are used to determine the optimal building group in key areas.

As for the estimation and analysis of surface temperature distribution, remote sensing images are widely used due to their coverage, spatial resolution, and periodicity. Merging techniques have been developed to downscale Landsat and MODIS images to balance spatial and temporal resolution (Bonafoni, 2016). Morphological methods can be applied to identify a Local Surface Urban Heat Island from Land Surface Temperature, providing a refined view of local hotspots.

The above research provides multiple methods for assessing the urban heat environment from different aspects and at different scales, and together provide the foundation of the framework described in this paper.

1.2 This study

This paper proposes a comprehensive framework that combines the assessment of the current urban heat environment, analysis of impervious surface, simulation of wind flow and formulation of spatial policies. The model contains four essential parts: 1) the morphological model retrieves land surface temperature from Landsat 7/8 ETM+ images and identifies Local Urban Heat Islands from its spatial pattern; 2) the geo-spatial model generates Local Climate Zones (LCZ) from the Digital Elevation Model, building database and land use database, and calculates the surface ventilation potential distribution; 3) the meteorological model simulates the local wind field at different air pressure levels, indicating potential passages for natural wind; 4) the fluid dynamics model aids optimization of building patterns in certain key areas and urban hotspots.

The model works as follows:

1) Land Surface Temperature (LST) is retrieved from Landsat 7/8 ETM+ images of the target area, which is then imported into MATLAB scripts that calculate the Multi-Scale Shape Index and local curvedness. These two parameters, together with a temperature threshold, are combined to find Local Urban Heat Islands, where MSSI is higher than 0.5 (indicating a higher temperature than surrounding pixels) and curvedness is higher than 0.05 (indicating an area that is large enough to be significant).
2) The Digital Elevation Model (DEM), building database and mesoscale meteorological data are imported into the Weather

Research and Forecast model, which generates local wind fields that contain three CSV data files, respectively representing a wind speed matrix for east-west vector, north-south vector and vertical vector. Data from the local weather station is used for explicating wind directions within the city. Potential natural wind paths are identified accordingly.

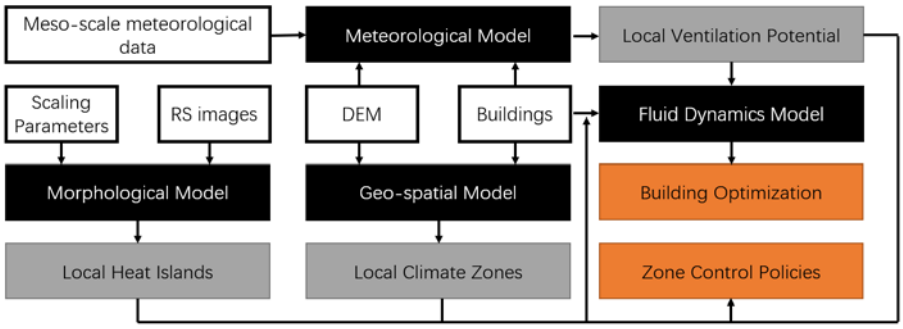

Figure 1. Workflow of The Model

3) The DEM, land surface and building database are imported into the GIS-based geo-spatial model that calculates numerous indicators related to local ventilation potential and local climate characteristics. Land pixels are given a potential ventilation index and LCZ codes.
4) Local ventilation potential and potential natural wind paths are combined to delineate areas with low ventilation potential but are on crucial positions of wind paths. Building models in such areas are altered into a variety of versions, which are then compared using Computational Fluid Dynamics (CFD) software so that an optimized version can be selected to support renewal plans. Unbuilt areas are tested under different construction scenarios so that the corresponding restrictions can be formulated.

Details of the model components will be introduced in the next chapter.

2. MODEL COMPONENTS

2.1 Morphological model

The morphological model imports Landsat images calculate latent Land Surface Temperature (LST) patterns and locates local urban heat islands on the MATLAB platform.

2.1.1 Retrieving latent LST

Due to its high spatial resolution, Landsat7 ETM+ is appropriate for urban studies and research relating to LST. Since they have only one thermal band, the classic Mono-window Algorithm is proposed to retrieve the land surface temperature (Qin, Karnieli, & Berliner, 2001), in which

$$T_{surface} = \{a(1-C-D) + [b(1-C-D) + C + D]T_{sensor} - DT_a\}/C$$

where $T_{surface}$ is the retrieved LST (°C), T_{sensor} is the sensor brightness temperature (K), T_a denotes effective mean atmospheric temperature (K), as

a and b are constants with a value of 67.4 and 0.46 respectively, while C and D are intermediate variables denoted as

$$C = \varepsilon\tau$$
$$D = (1-\tau)[1+(1-\varepsilon)\tau]$$

Where ε and τ are land surface emittance and atmospheric transmittance. The average estimation error is 1.1 °C if the inaccuracy of ε, τ and T_a are considered (Zhan, Meng, & Xiao, 2015).

2.1.2 Locating local urban heat island

Two parameters are then calculated for each pixel on latent LST, respectively the Multi-Scale Shape Index (MSSI) and curvedness.

By projecting the LST pattern $f(s)$ to scale space through

$$S(f(s),\sigma) = f(s) * k(s-u,\sigma) = \int\_s\^0 f(u)k(s-u,\sigma)du$$

Where $k(\cdot,\cdot)$ is the Gaussian kernel, with different smoothing magnitude σ centered at each location u on the surface s. A normalized distance is presented as

$$d = (D(f,\sigma))/\sigma = \|S(f,\sigma) - f\|\^2/\sigma$$

and the optima scale σ can be identified by the maxima of d.

The MSSI is then evaluated as the SI at each point at the optimal scale, where the SI of a point on a surface is represented as (Koenderink & van Doorn, 1992).

$$SI = \pi/2\, arctan\,(\kappa\_2+\kappa\_1)/(\kappa\_2-\kappa\_1), SI \in [-1,1]$$

Where κ_1 and κ_2 are the principle curvatures evaluated from a noise continuous latent LST surface through eigenvalues of the Hessian matrix. How it represents the relationship of a point with its surroundings is shown in *Figure 2*.

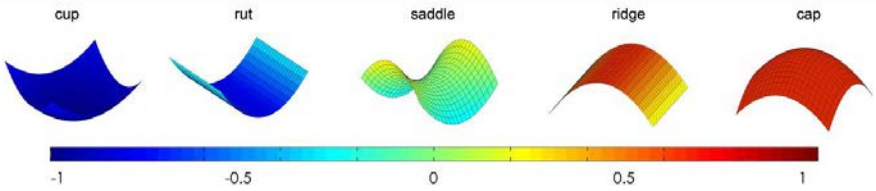

Figure 2. The Surface Morphology in The Range of Shape Index

2.2 Meteorological model

The meteorological model uses mesoscale meteorological data and building data to simulate wind speed and wind direction to a refined spatial resolution using the Weather Research and Forecast (WRF) model. Previous research found that WRF, at its best, can run on kilometer-level resolution (Jiménez et al., 2010; Yang, Zhang, & Qian, 2012). Hence, 1km is chosen as the spatial resolution for the simulation.

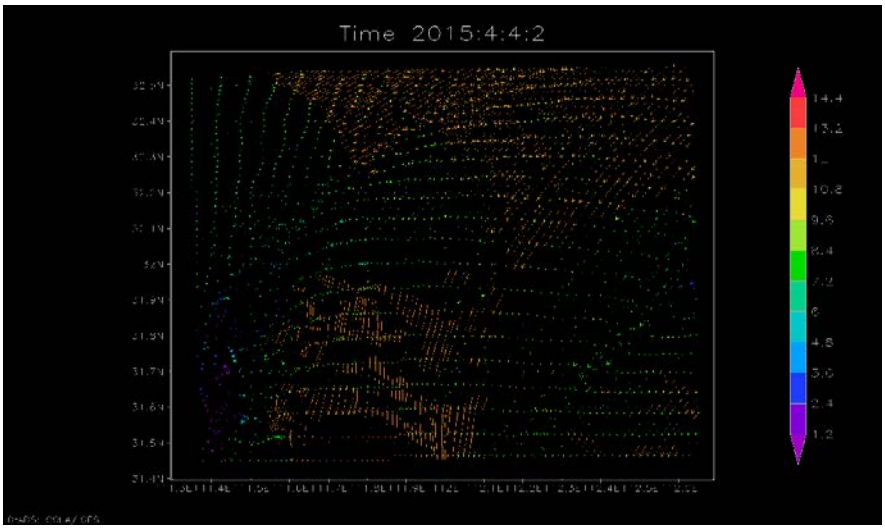

Figure 3. An Example of The WRF Simulation Result, with Vertical Speed Emitted.

WRF is a numerical weather prediction (NWP) and atmospheric simulation system designed for both research and operational applications (Skamarock et al., 2005). To incorporate the urban surface and variables into the simulation process, an urban canopy model (UCM) originally developed by Kusaka et al. (2001) and Kusaka & Kimura (2004) and later modified by Chen et al., (2002), is coupled with the WRF model. The UCM estimates the surface temperature and heat fluxes from the surfaces of the roof, wall and road, as well as calculating the momentum exchange between the urban surface and the atmosphere (Skamarock et al., 2005).

The SLAB model, as one of the UCM surface layer schemes, is applied in this study. Urban geometry is represented as some surface parameters, such as roughness length, albedo, thermal inertia and moisture availability. As anthropogenic heat is not measured and there is no anthropogenic heat emission consideration in the SLAB scheme, this scheme is selected to simulate the overall atmospheric environment at the mesoscale.

Simulations in this study are done in WRF, version 3.6, and all the parameters used in the SLAB model are listed in *Table 1*. An example of the WRF simulation result is shown in *Figure 3*.

Table 1. Parameters Used in The SLAB model

Parameters	Value
Roughness Length (m)	0.80
Moisture Availability (-)	0.10
Albedo (-)	0.15
Emissivity (-)	0.88
Thermal Inertia ($Js^{-1}K^{-2}m^{-4}$)	3.52×10^{6}

2.3 Geo-spatial model

The geo-spatial model utilizes DEM and building data to retrieve Local Climate Zones and key indicators in evaluating local ventilation potential. The process is scripted as a Python program and runs on the ArcGIS 10.2 platform.

2.3.1 Ventilation potential

The macroscopic wind environment and overall ventilation potential of a city are dependent on its climatic and geographic conditions, but ventilation capabilities within the city are also largely determined by its built environment. Microscopic simulation with Computational Fluid Dynamics has proven that various factors exert their influence, including the overall density of buildings，building height, the area density of buildings facing the orientation of winds (i.e., Front Area Density, FAD), and open space provided by squares, green space, and roads (Yin & Zhan, 2016).

To quantify these factors, a set of indicators, as shown in *Table 2*, are defined to describe the built environment: Building Density, Height-Width Ratio, Front Area Density, Absolute Degree of Folding, Porosity, Building Height Variety, and Building Group Proximity. Additionally, another set of indicators describe the segments of the local road network: Road Width, Road Height-Width Ratio, and Wind Orientation Coherence. Among these indicators, FAD and Wind Orientation Coherence are related to the result of macroscopic wind environment simulation, where local wind direction is generated. All indicators can be calculated from the city geodatabase in the ArcGIS environment, to which the Analytic Hierarchy Process (AHP) is applied to determine the weights of various indicators for buildings.

Table 2. Indicators in Built-Up Environment Analysis

Indicators	Definition	Implication on Ventilation	Data Source	Resolution
Building Density	Building Base Area / Raster Unit Area	Relates to ventilation levels on walking height	Building Survey of Wuhan, 2012	500m
Front Area Density	Total Front Area / Raster Unit Area	Relates to ventilation levels on walking height	Building Survey of Wuhan, 2012	500m
Degree of Folding	(Sum of (Building Base Area * Building Height)) / Raster Unit Area	Relates to average wind velocity	Building Survey of Wuhan, 2012	500m
Degree of Porosity	(Maximum Building Height*Raster Unit Area - Total Building Volume) / (Maximum Building Height * Raster Unit Area)	Relates to open space available for air flows	Building Survey of Wuhan, 2012	500m
Building Group Height Deviation	Standard Deviation of Building Heights in the Raster Unit	Relates to front area turbulence and wind velocity	Building Survey of Wuhan, 2012	500m
Road Height-Width Ratio	(Average Height of Correspondent Buildings) / (Distance Between Correspondent Buildings)	Relates to fraction resistance against winds and secondary air flows generated by high-rise buildings	Building Survey of Wuhan, 2012	By vector polygons

Indicators	Definition	Implication on Ventilation	Data Source	Resolution
Building Group Proximity	Distance to the Nearest Building	Relates to open space available for air flows	Building Survey of Wuhan, 2012	By vector polygons

Source: Yin & Zhan, 2016

2.3.2 Local Climate Zones

The LCZ is a framework proposed recently that describes the response of a certain area to meteorological factors, validated through circling places with radii of hundreds of meters in a few different cities. In this study, the target city is classified into climate zones with homogenous climate responses based on a variety of indicators, so that climate behavior at the local scale can be distinguished (Stone, Vargo, & Habeeb, 2012).

Indicators, shown in *Table 3*, are selected to reflect the meteorological properties of the land surface factors. They are considered as properties of a certain area of the land surface, which can be taken as a multi-dimensional vector for each 500m*500m pixel. The K-means clustering is applied to avoid empirical values in partitioning the observation artificially. Regarding the pixels as n observations, for each observation, the property is a d dimensional vector $\boldsymbol{p}$. To separate the pixels into k sets, the clustering process attempts to find

$$arg\ min \sum_{i=1}^{k} \sum \|\boldsymbol{p} - \boldsymbol{\mu}_i\|^2$$

where μ_i is the mean of cluster i.

Table 3. Indicators Used for LCZs Classification

Indicators	Definition	Meteorological Implication	Data Source	Resolution
Sky View Factor	The fraction of sky visible from a certain point of the land surface.	Response actively to solar radiation and heat dissipation.	Building Survey of Wuhan, 2012	500m
Building Surface Fraction	The fraction of building a footprint in a curtain land unit.	Relates to surface run-off and moisture.	Building Survey of Wuhan, 2013	500m
Impervious Surface Fraction	Fraction of impervious surface.	Relates to surface run-off and moisture.	Landsat ETM+	500m
Pervious Surface Fraction	The fraction of pervious surfaces such as vegetation and water.	Relates to surface run-off and moisture.	Landsat ETM+	500m
Vegetation Index	Coverage of vegetation.	Relates to energy and water transitions.	Landsat ETM+	500m

Indicators	Definition	Meteorological Implication	Data Source	Resolution
Water Index	Coverage of water bodies.	Relates to energy and water transitions.	Landsat ETM+	500m
The height of the Roughness Elements	The height of construction and natural relief.	Affects the airflow and heat dissipation within an urban area.	Building Survey of Wuhan, 2012	500m
Terrain Roughness Class	Classification of roughness height.	Affects the airflow and heat dissipation within an urban area.	Building Survey of Wuhan, 2013	500m
Digital Elevation Model	Depicts the morphological property of relief.	Affects the airflow and heat dissipation within an urban area.	DEM, 2012	500m
Surface Admittance	The capability to absorb and emit energy.	The efficiency of transmitting energy.	Landsat ETM+	500m
Surface Albedo	The overall reflectance.	The efficiency of reflecting short wave radiation.	Landsat ETM+	500m

Source: Jiong Wang, Zhan, & Guo, 2015

2.4 Fluid Dynamic Model

In wind path planning, certain neighborhoods or building groups may significantly affect the neighborhoods and their surroundings by important blockading paths of natural wind (Ng, 2009). With the help of Computational Fluid Dynamics (CFD) simulations, such influencing variables can be quantified and visualized with the three-dimensional model of the neighborhoods in question (Guo & Zhan, 2015). For the neighborhoods themselves, analysis and optimization of the microscopic wind environment consist of three steps: cognitive space delineation, wind environment optimization, and analysis and validation of wind environment optimization.

In cognitive space analysis, space syntax is applied to the CAD layout plan of the target neighborhoods to calculate the spatial distribution of the Integration Index, which represents the accessibility and potential intensity of activities in a certain space. Thus, areas with a high Integration Index are to be given higher priority in wind environment optimization.

3. PLANNING PRACTICES

3.1 Study area

Two Chinese cities, Wuhan and Fuzhou, are selected as case studies. Wuhan is located in central China, and Fuzhou is located on the southeast coast (*Figure 4*). Both are dense cities suffering severe heat in summer, known as Chinese “stove cities.” Wuhan is in the east of the Jiang-Han plain, with very even terrain but many large lakes and two major rivers

crossing the city, where 25.79% of the administrative area is water. Fuzhou is on a typical estuary basin, surrounded by hills and mountains. They are both Subtropical monsoon climates, but wind resources are different due to their specific geographical environments. Following is an introduction to the analysis and planning results of these two cities.

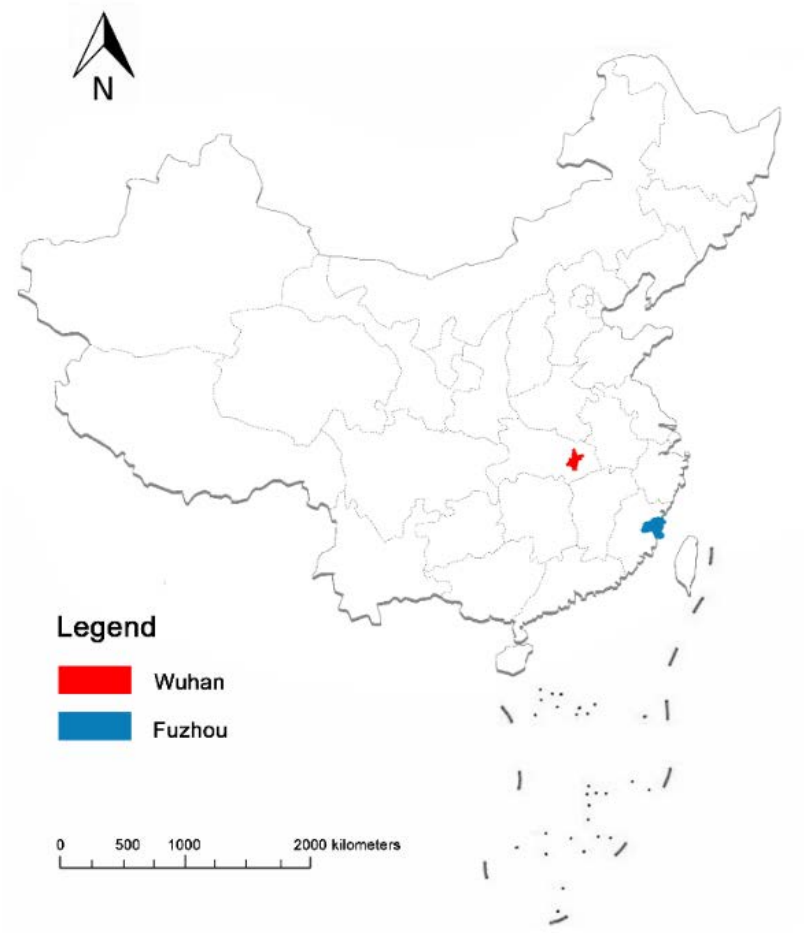

Figure 4. Study Area

3.2 Data

In these two cases, all LST retrieval is based on Landsat7 ETM+. Considering the quality of remote sensing images and its compatibility with other source data, images were chosen for August 8, 2013, for Wuhan and June 14, 2014, for Fuzhou. As the initial and boundary conditions of the WRF simulations, the NCEP Final (FNL) Analysis data, taken on the same dates as Landsat7, were downloaded and utilized. The SLAB parameters are addressed in *Table 1* as the default. Other data includes building vector datasets, separately produced in 2012 for Wuhan and 2014 for Fuzhou, meteorological station positions, and yearly weather recordings for each station in the same year as the building datasets respectively.

3.3 Result and analysis

The LST distributions at 10 am are displayed in *Figure 5* and *Figure 6.* The highest LST in Wuhan is around 47.6ºC, while in Fuzhou the value is up to 50ºC. The water bodies in both cities display the lowest temperatures,

as well as some mountain valleys and large green lands. Within the boundary of the urban area in Wuhan, the average LST in the built-up area reached above 43ºC, where most urban citizens live and work. The thermal conditions in the north of Fuzhou seem severe as well, where the average built-up LST is above 45ºC. Since the temperature differences between urban areas and surrounding places are 25ºC and 35ºC, the urban heat islands in Wuhan and Fuzhou are serious enough to require adaptation and mitigation response. As described in the introduction, the excessive heat in urban areas can be optimized by air circulation; therefore, the urban ventilation path is extremely important.

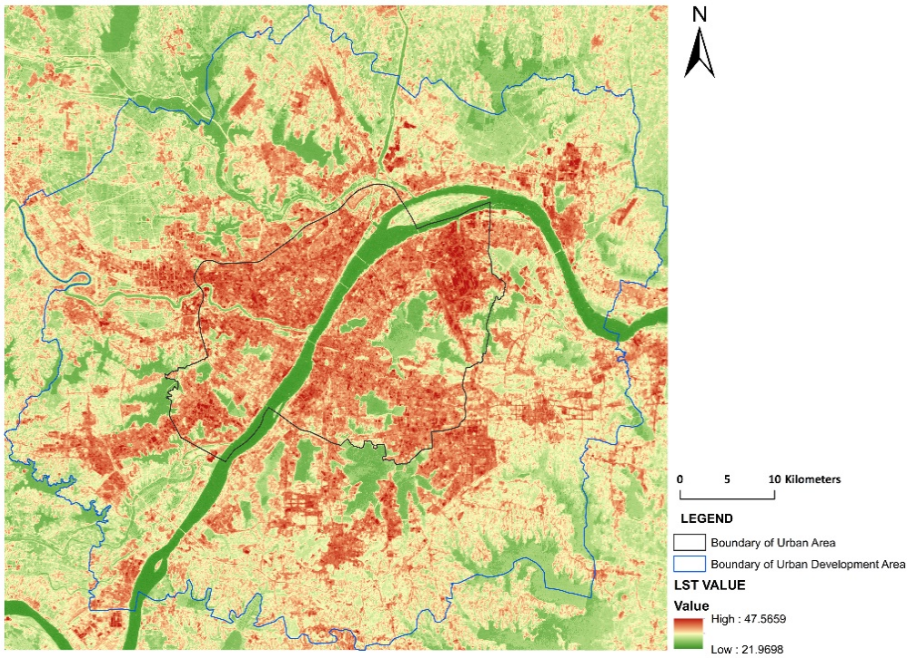

Figure 5. LST Distribution in Wuhan from Landsat7 ETM+, August 8th, 2013

The air flow within urban areas is originally based on a natural wind source created by pressure and terrain differences. For these cases, WRF is used to discover the natural wind sources of Wuhan and Fuzhou, both qualitatively and quantitatively.

Typical hours were chosen to represent the daytime and night-time situations respectively. According to *Figure 7* and *Figure 8*, the natural wind resource in Wuhan generally comes from the southwest, where there is a river canyon between mountains. As Wuhan lies in the Jiang-Han plain and is surrounded by higher terrain, the speed of natural wind near the surface may reach 10 meters per second during the day and 7 meters per second at night. The situation in Fuzhou is more complicated because Fuzhou lies on the coast of the East China Sea. On the basis of simulation results, the main wind resource comes from the south and east of Fuzhou, respectively major mountains and sea coast. The direction changes a little at night as air mainly flows from the land to the sea due to the heat capacity of the ocean. The SLAB module considers urban areas coarsely and naively; thus, the results may only reflect the wind source patterns. Therefore, a more detailed depiction of the wind path within urban areas requires further analyses based on data from other sources.

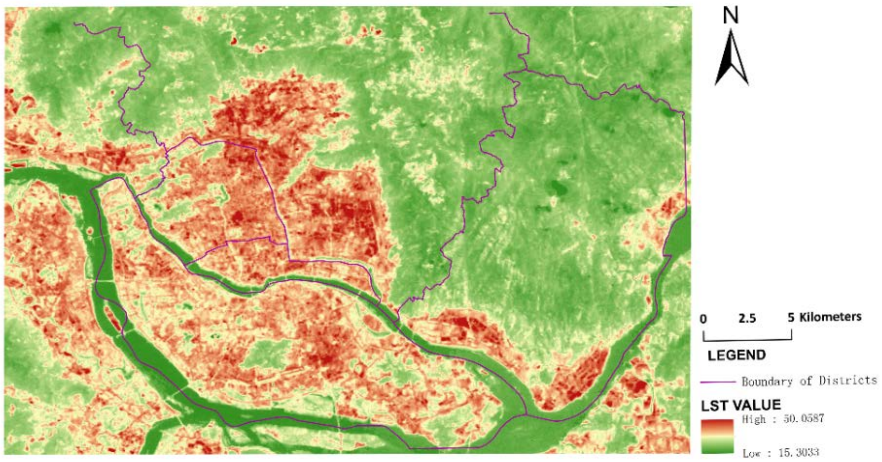

Figure 6. LST Distribution in Fuzhou from Landsat7 ETM+, June 14th, 2014

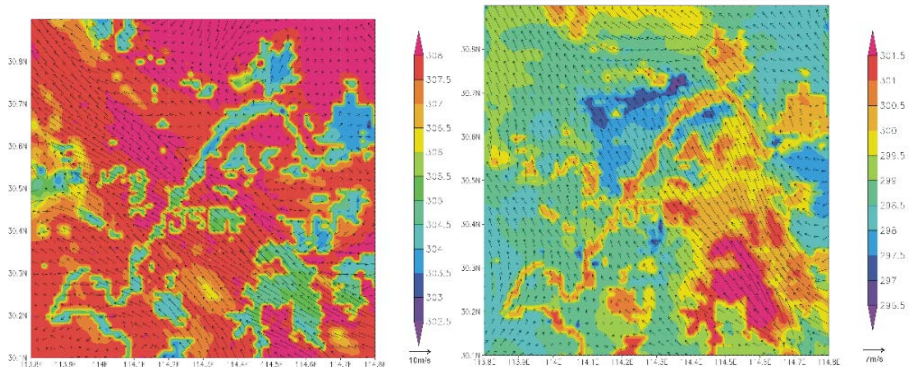

Figure 7. WRF Simulation in Wuhan. Left: Daytime; Right: Night-time

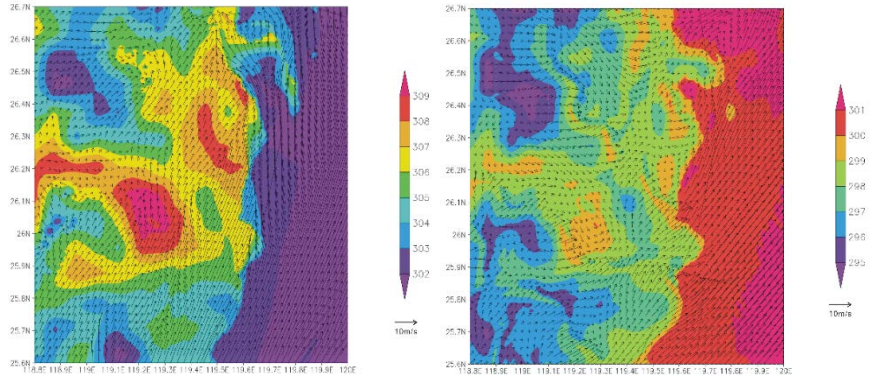

Figure 8. WRF Simulation in Fuzhou. Left: Daytime; Right: Night-time

In order to accurately depict ventilation conditions inside the urban areas, the wind rose analysis is employed. *Figure 9* and *Figure 10* show the wind rose of each weather station for Wuhan and Fuzhou. *Figure 9* shows that the main wind direction in Wuhan is from southwest to northeast, the same direction as the Yangtze River, however, small variations exist at the local scale, especially around large water bodies, such as the Yangtze River, East Lake, Moshui Lake, and South Lake. Due to the impact of river breeze and lake breeze, the wind direction of the weather stations around these lakes generally flows from the water areas to the land. Additionally, the wind speed around the water areas is generally larger than other places. *Figure 10* indicates that the predominant wind direction in Fuzhou is from

southeast to northwest, mainly affected by the sea breeze, but as Fuzhou is surrounded by mountains, mountain-valley wind resources are also very abundant, especially from the mountains to the north and the south of the city. As a result, the wind direction near the city center mainly corresponds with the sea breeze, but the wind direction near the edge of the urban areas is mainly influenced by the mountain-valley breeze. The wind speed near the city center is significantly slower than the city periphery due to high-intensity construction inside the city.

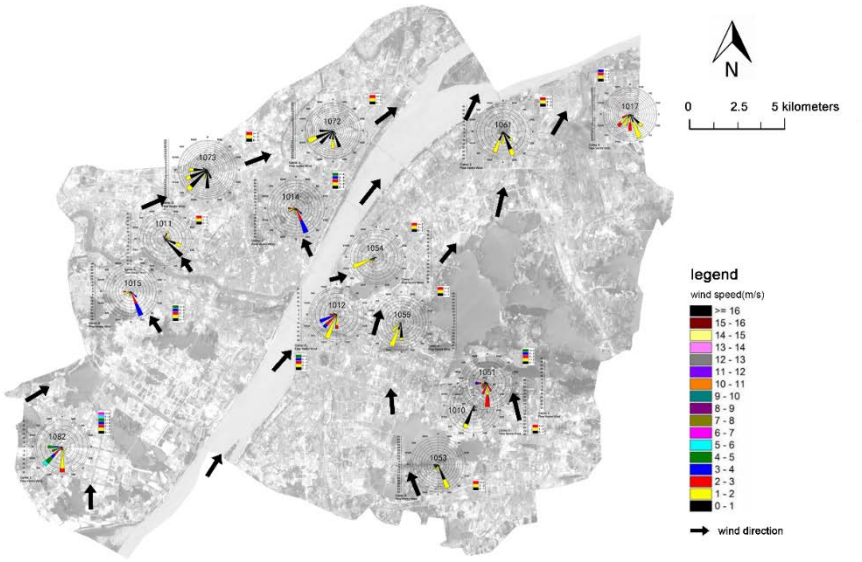

Figure 9. Wind Rose Analysis of Wuhan

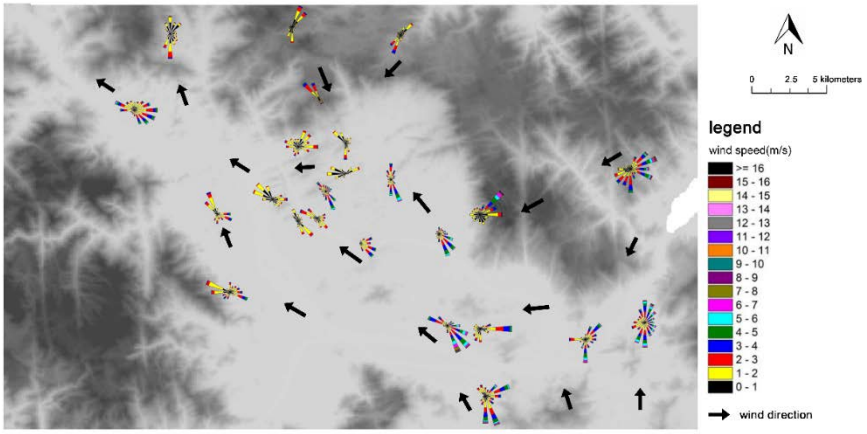

Figure 10. Wind Rose Analysis of Fuzhou

3.4 Building environment analysis

To identify intra-urban construction characteristics, to excavate the potential ventilation path, the local ventilation potential is calculated. Here the Frontal area index (λf) is taken as an example. The λf distribution in Wuhan (*Figure 11*) shows that the overall λf is high in the city center areas, which means high-intensity construction and bad wind permeability. Nonetheless, there are still some spaces with low λf that can be beneficial to the local wind environment. These spaces are usually water areas, open spaces, green spaces, and wide roads. Also, once these spaces are strung

together, there would be a good intra-urban ventilation path. *Figure 12* shows that areas with higher λf in Fuzhou are mainly located in the north, and especially in the city center. The building density in the south is significantly lower. Owing to geographical features, Fuzhou has almost no natural water bodies and hills inside the city, leading to massive, intensive construction. The only area with lower λf in northern Fuzhou should be maintained so as to prevent ventilation conditions from further deteriorating.

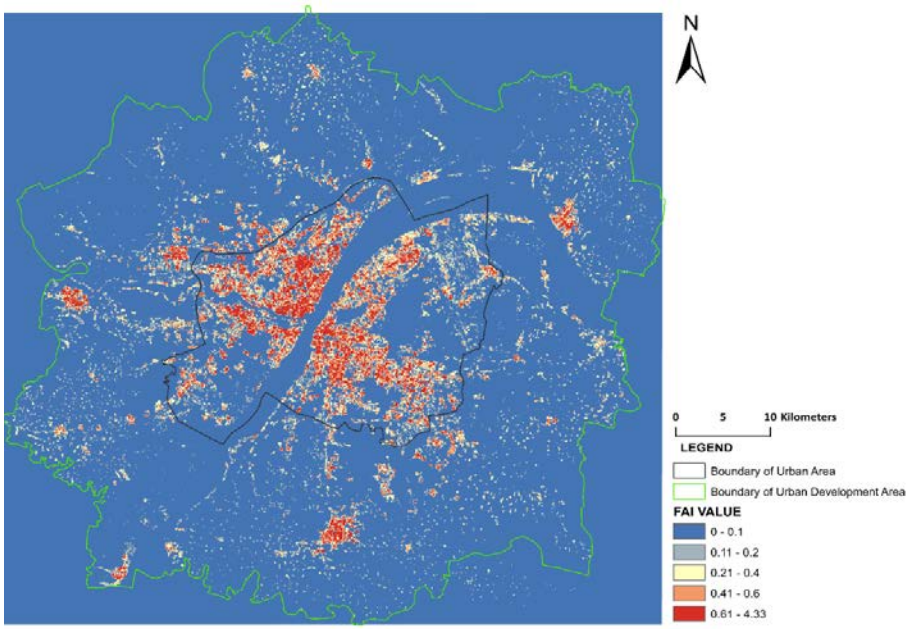

Figure 11. FAI Analysis of Wuhan

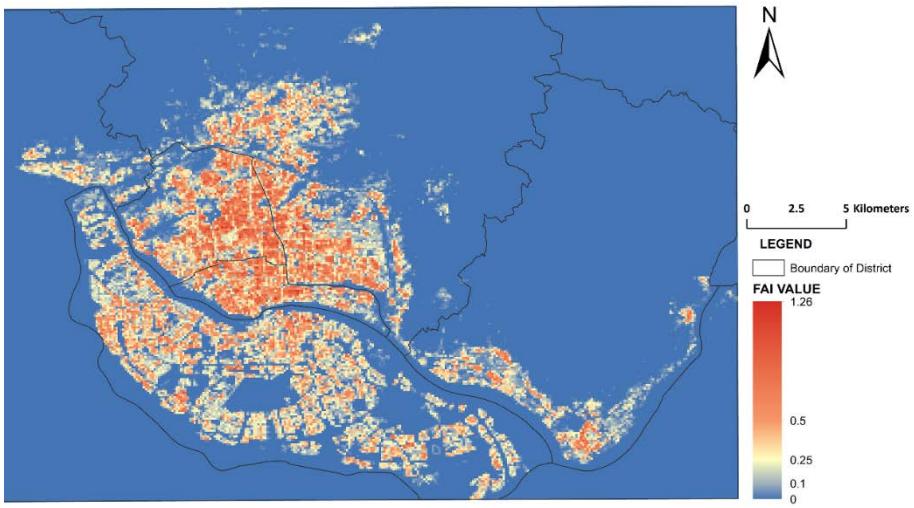

Figure 12. FAI analysis of Fuzhou

With previous analysis of wind resources, integrating urban meteorological data and the built environment, wind path maps were generated for both cities. Wind path maps reflect where the wind comes from, as well as how air circulates within cities. In Wuhan, the Yangtze River is a major wind path running through the city. The intra-urban wind path comes from the combination of meteorological data analysis and FAI analysis. Fuzhou is distinguished from Wuhan by its more abundant wind resources, both from mountain-valley breeze and sea-land breeze, hence the

situation in Fuzhou may be more complicated than Wuhan. The intra-urban wind path in Fuzhou flows mainly in the direction of the Minjiang River.

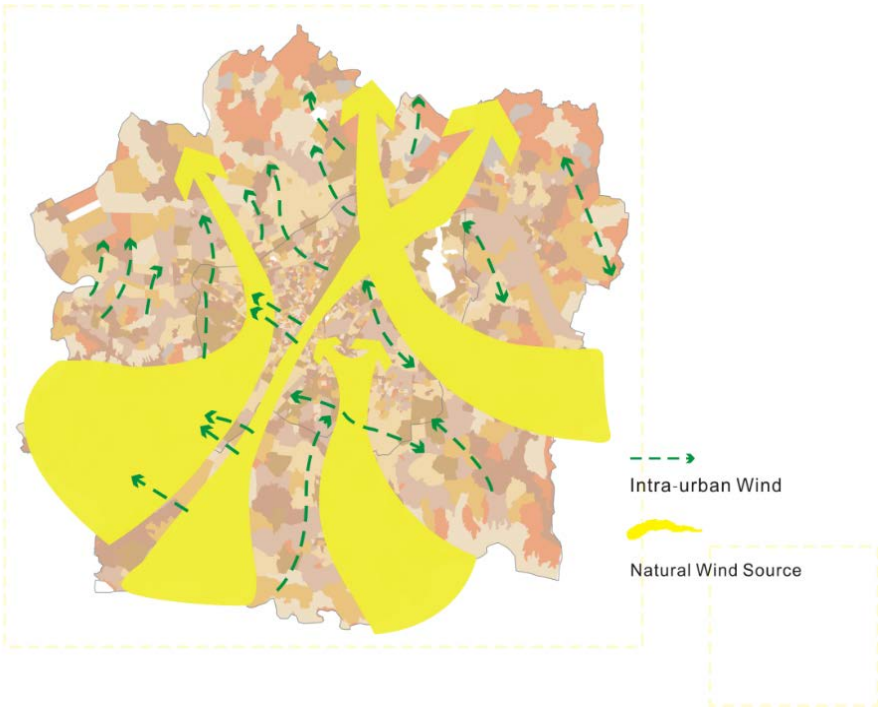

Figure 13. Wind Path Mapping in Wuhan

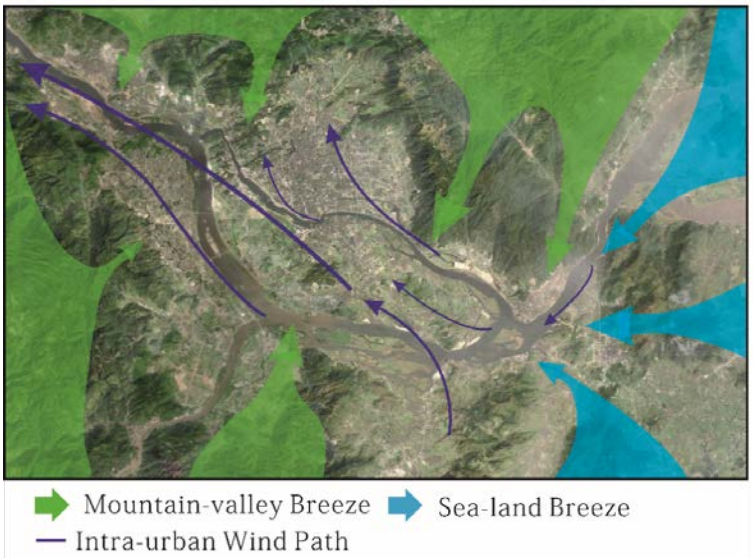

Figure 14. Wind Path Mapping in Fuzhou

3.5 Planning implementation

Even with the current vast amount of urban climate research, its application to urban planning is still very limited (Eliasson, 1996). This paper has formulated strategies that should be taken to: 1) protect urban wind entrances, and 2) give some planning guidelines to control the spatial form of ventilation paths, thus preventing the urban heat environment from further deteriorating. The former ensures the natural wind resource can blow into urban areas, whereas the latter can facilitate the passing of wind through more places to accelerate the air flow and carry off excessive heat.

The width and direction of the ventilation path and the height and configuration of buildings around the path are the main controllable indicators. Besides this, street furniture, billboards, and street plants should be arranged in accordance with the wind direction to reduce wind obstruction.

4. CONCLUSION

Now that the ecological environment has become a public concern, planners should incorporate ecological and sustainable considerations into urban studies, planning and policy making. This research combines remote sensing, geographical information technologies and meteorological modeling, not only to explore measures to examine and evaluate the urban heat environment, but also to provide a better scientific basis for urban wind path planning. Due to the complexity of air circulation and ventilation, the analysis method of the urban ventilation corridor needs to be further improved and the research about how to explicitly locate potential air paths still awaits exploration. Further developments, such as how to explicitly locate and extract potential air paths automatically and how to improve the urban ventilation environment on the basis of inventory planning, is of great interest to us.

5. DISCUSSION

The workflow in this paper provides new insight and a novel approach to exploring urban ventilation paths. To some extent, it provides a spatial and quantifiable foundation for decision-making. There are, however, some limitations worthy of discussion.

1) The linkage between different model components needs to be further strengthened. RS technology was employed to analyze the UHI phenomenon; the meteorological model was involved in locating wind resources, and GIS was used to analyze the urban land surface roughness and local climate. The three technologies are based on different platforms and data, so the analysis of each level lacks strong continuity and progression.

2) The workflow is more feasible for current wind tunnel excavation, so it is more applicable to cities that have almost completed urban construction, meaning dense urban areas. As for cities undergoing rapid urbanization, this workflow is not suitable for pre-planning urban ventilation paths because the data needed in this workflow is almost entirely based on the current level of development in the built area. However, exploring how to pre-plan urban ventilation for these cities is very necessary as it can help to mitigate future bad situations.

ACKNOWLEDGEMENT

This research is supported by the National Natural Science Foundation of China (No. 41331175, 51378399).

REFERENCES

Bonafoni, S. (2016). "Downscaling of Landsat and MODIS land surface temperature over the heterogeneous urban area of Milan", *IEEE Journal of Selected Topics in Applied Earth Observations and Remote Sensing*, *9*(5), 2019–2027.

Cai, M., Ren, C., Xu, Y., Lau, K. K. L., & Wang, R. (2018). "Investigating the relationship between local climate zone and land surface temperature using an improved WUDAPT methodology – A case study of Yangtze River Delta, China", *Urban Climate*, *24*, 485–502. https://doi.org/10.1016/j.uclim.2017.05.010

Chen, Y. H., Li, X. B., Shi, P. J., & He, C. Y. (2002). "Study on spatial pattern of urban heat environment in Shanghai city", *Scientia Geographica Sinica*, *22*(3), 317–323.

Eliasson, I. (1996). "Intra-urban nocturnal temperature differences: A multivariate approach", *Climate Research*, *7*(1), 21–30. https://doi.org/10.3354/cr007021

Feng, X., Sa, L., Li, F., Li, M., Zhou, Z., & Yuan, L. (2016). "The Simulation on Xi'an's Urban Heat Environment Based on Ca-Markov Model", *Journal of Xian University of Architecture & Technology*, *48*(5), 731–737.

Golden, J. S. (2004). "The Built Environment Induced Urban Heat Island Effect in Rapidly Urbanizing Arid Regions – A Sustainable Urban Engineering Complexity", *Environmental Sciences*, *1*(4), 321–349. https://doi.org/10.1080/15693430412331291698

Guo, H., & Zhan, Q. (2015). "Optimization of wind environment of cognitive space based on space syntax and computer numerical simulation",.

Ishida, H., Tsumura, I., & Takagi, M. (1997). *Research Report Collection of Architectural Institute of Japan. Case Study on the Air Temperature Distribution and Wind Path in Asahikawa City: For Climatic Thermo-Scape Urban-Design*, Hokkaido.

Jiménez, P. A., González-Rouco, J. F., García-Bustamante, E., Navarro, J., Montávez, J. P., De Arellano, J. V. G., … Muñoz-Roldan, A. (2010). "Surface wind regionalization over complex terrain: Evaluation and analysis of a high-resolution WRF simulation", *Journal of Applied Meteorology and Climatology*, *49*(2), 268–287. https://doi.org/10.1175/2009JAMC2175.1

Koenderink, J. J., & van Doorn, A. J. (1992). "Surface shape and curvature scales", *Image and Vision Computing*, *10*(8), 557–564. https://doi.org/10.1016/0262-8856(92)90076-F

Kusaka, H., Hiroaki, K., Yokohiro, K., & Fujio, K. (2001). "A Simple Single-Layer Urban Canopy Model for Atmospheric Models : Comparison with Multi-Layer and Slab Models", *Boundary-Layer Meteorology*, *101*(3), 329–358.

Kusaka, H., & Kimura, F. (2004). "Coupling a Single-Layer Urban Canopy Model with a Simple Atmospheric Model: Impact on Urban Heat Island Simulation for an Idealized Case", *Journal of the Meteorological Society of Japan*, *82*(1), 67–80. https://doi.org/10.2151/jmsj.82.67

Li, J., & Rong, Y. (2014). "Construction of Urban Wind Paths in Wuhan and Its Guidance on Design and Planning Control", *Planners*, (8), 115–120.

Luber, G., & McGeehin, M. (2008). "Climate Change and Extreme Heat Events", *American Journal of Preventive Medicine*, *35*(5), 429–435. https://doi.org/10.1016/j.amepre.2008.08.021

Medina-Ramón, M., Zanobetti, A., Cavanagh, D. P., & Schwartz, J. (2006). "Extreme temperatures and mortality: Assessing effect modification by personal characteristics and specific cause of death in a multi-city case-only analysis", *Environmental Health Perspectives*, *114*(9), 1331–1336. https://doi.org/10.1289/ehp.9074

Ng, E. (2009). "Policies and technical guidelines for urban planning of high-density cities - air ventilation assessment (AVA) of Hong Kong", *Building and Environment*, *44*(7), 1478–1488. https://doi.org/10.1016/j.buildenv.2008.06.013

Qin, Z., Karnieli, A., & Berliner, P. (2001). "A mono-window algorithm for retrieving land surface temperature from Landsat TM data and its application to the Israel-Egypt border region", *International Journal of Remote Sensing*, *22*(18), 3719–3746.

Skamarock, W. C., Klemp, J. B., Dudhi, J., Gill, D. O., Barker, D. M., Duda, M. G., … Powers, J. G. (2005). *A Description of the Advanced Research WRF Version 2*, *Technical Report*, Boulder, Colorado, USA. https://doi.org/10.5065/D6DZ069T

Stewart, I. D., & Oke, T. R. (2012). "Local climate zones for urban temperature studies", *Bulletin of the American Meteorological Society*, *93*(12), 1879–1900. https://doi.org/10.1175/BAMS-D-11-00019.1

Stone, B., Vargo, J., & Habeeb, D. (2012). "Managing climate change in cities: Will climate action plans work?", *Landscape and Urban Planning*, *107*(3), 263–271. https://doi.org/10.1016/j.landurbplan.2012.05.014

Wang, J., Zhan, Q., & Guo, H. (2015). "The morphology, dynamics and potential hotspots of land surface temperature at a local scale in urban areas", *Remote Sensing*, *8*(1),. https://doi.org/10.3390/rs8010018

Wang, J., Zhan, Q., & Xiao, Y. (2015). "Hierarchical climate zone as a tool for spatial planning–Case study of Wuhan, China", In: *The International Conference on Computers in Urban Planning and Urban Management 2015*,.

Xu, H. (2010). "Analysis of Impervious Surface and its Impact on Urban Heat Environment using the Normalized Difference Impervious Surface Index (NDISI)", *Photogrammetric Engineering & Remote Sensing*, *76*(5), 557–565. https://doi.org/10.14358/PERS.76.5.557

Xue, J. (2007). "Spatial characteristics and dynamic simulations of urban heat environment of cities in Pearl River Delta", *Acta Ecologica Sinica/Shengtai Xuebao*, *27*(4),.

Yang, B., Zhang, Y., & Qian, Y. (2012). "Simulation of urban climate with high-resolution WRF model: A case study in Nanjing, China", *Asia-Pacific Journal of Atmospheric Sciences*, *48*(3), 227–241.

Yin, J., & Zhan, Q. (2016). "The Relationship between Ventilation and Urban Morphology Based on the Method of Morphology – Taking Wuhan as an Example", *Environmental Protection*, *44*(22),.

Zhan, Q., Meng, F., & Xiao, Y. (2015). "Exploring the relationships between land surface temperature, ground coverage ratio and building volume density in an urbanized envronment", *International Archives of the Photogrammetry, Remote Sensing and Spatial Information Sciences - ISPRS Archives*, *40*(7W3), 255–260. https://doi.org/10.5194/isprsarchives-XL-7-W3-255-2015